C.L. SCHILLER[1,2,✉]
H. BOZEM[1]
C. GURK[1]
U. PARCHATKA[1]
R. KÖNIGSTEDT[1]
G.W. HARRIS[2]
J. LELIEVELD[1]
H. FISCHER[1]

Applications of quantum cascade lasers for sensitive trace gas measurements of CO, CH_4, N_2O and HCHO

[1] Max-Planck Institut für Chemie, Abteilung Luftchemie, P.O. Box 3060, 55020 Mainz, Germany
[2] Centre for Atmospheric Chemistry, York University, 4700 Keele Street, Toronto, Ontario, M3J 1P3, Canada

ABSTRACT We describe here a sensitive quantum cascade laser absorption spectrometer (QCLAS) employed for aircraft based measurements during the GABRIEL 2005 and HOOVER 2006 and 2007 campaigns. This 3-channel instrument measures CO, HCHO, CH_4 and N_2O using a 64-m path double corner cube White cell. Performance of the instrument was examined for the four species and precisions for CO, N_2O and CH_4 were measured in the field to be 0.5, 0.5 and 0.7% respectively (2σ). The 1σ detection limit for HCHO was ~500 pptv for a 2 s average, while signal averaging of the HCHO over a 2 min time interval resulted in a 150 pptv detection limit with a duty cycle of 60%.

PACS 82.80.Gk; 07.88.+y; 42.62.-b; 92.60.H-

1 Introduction

Tunable diode laser absorption spectroscopy (TDLAS) in the mid-infrared has widespread applications in the field of atmospheric research [1–8]. In this technique a monochromatic laser in the mid-infrared is tuned across a rotational-vibrational line of a molecule of interest. Narrowing the line by pressure reduction (~ 50 mbar) has minimal effect on the line center cross section and thus maintains the sensitivity while reducing the possible interferences by overlap of other species. Use of a multi-pass reflection cell can yield sub-ppbv detection limits for many smaller molecules of atmospheric relevance including HCHO, H_2O_2, NO_2, HNO_3, NH_3, OCS, HCl, C_2H_2, HONO, CO, CH_4 and N_2O [9–12]. This corresponds to minimum optical densities of 10^{-6}–10^{-5} with time resolutions ranging from seconds to minutes.

Until recently, TDLAS used lead chalcogenide lasers but recently advances in the sensitivity and stability of the technique have been increased by employing quantum cascade (QC) lasers [13–15]. Working in the mid-infrared in continuous-wave (cw) operation requires cooling of the lasers below 210 K. Higher output powers are obtained by cooling to liquid nitrogen temperatures. Laser and detector noise as well as optical noise due to unstable optical fringes generally limit TDLAS utilizing lead-salt lasers. However, due to the higher powers of the QC laser (25–150 mW), detector noise is no longer an issue and pressure and temperature stability play a larger role in the precision and detection limits. QC lasers, with their higher powers and their stability have been shown to reduce noise by about a factor of three compared to their lead-salt counterparts [14].

In the atmosphere, measurement of CO, N_2O and CH_4 can be important in deducing air mass origins and tracer transport pathways, HCHO is important in understanding the chemical mechanisms and oxidative capacity of the atmosphere, while all of these molecules are important for validation of chemical transport models. Ambient mixing ratios of CO and CH_4 are much higher than HCHO and considerable precision is often required to detect small changes in mixing ratio and subtle changes in air mass origin. Formaldehyde is an important molecule as both an intermediate in the oxidation of volatile organic compounds (VOCs) and for the production of radicals through photolysis. Formaldehyde is an oxidation product of both anthropogenic and biogenic hydrocarbons, but it may also be directly emitted in combustion processes, e.g. biomass burning events. Once in the atmosphere, formaldehyde may be lost through both wet and dry deposition, however its primary loss mechanism is through photolysis or reaction with radicals. The photolysis of formaldehyde partly results in the production of HO_2, which in the presence of NO_x may lead to significant OH and ozone production. Under low light conditions, such as mornings, evenings and winter months, formaldehyde may rival ozone photolysis as a source of the hydroxyl radical via its production of HO_2 [16]. Although mixing ratios of formaldehyde can be 10s of ppbv in urban settings, mixing ratios found in rural areas tend to be less than 2.5 ppbv. In remote areas and the free troposphere formaldehyde mixing ratios are dominated by the oxidation of methane resulting in formaldehyde mixing ratios often of the order of a few hundred parts per trillion by volume (pptv).

Measurements of HCHO using tunable diode laser absorption spectroscopy (TDLAS) were first reported in the early 1980s by utilizing the lead-salt lasers [8]. Due to the limits in the power, noise and stability of the lead salt lasers, detection limits were limited to ~ 200 pptv for ~ 30 min averages [8, 17].

In this paper we will present the capabilities of our airborne TRISTAR system to measure CO, HCHO, CH_4 and N_2O. Data collected during GABRIEL 2005 (Guyanas

Atmosphere–Biosphere Exchange and Radicals Intensive Experiment with the Learjet) and HOOVER 2006 and 2007 (HO_x over Europe) will be used to demonstrate the abilities of this system. Performance of the instrument during portions of three field experiments will be discussed. The goal of the GABRIEL flights was to examine the oxidation of isoprene emitted from the tropical rain forest, while the goal for HOOVER is to probe the background atmosphere and study the oxidative capacity of the upper troposphere over Europe.

GABRIEL was an airborne campaign consisting of ten 3.5–4 h flights in Suriname during October 2005. Suriname is located on the north east coast of South America. To the south and west lies the Amazon rainforest, to the east a tropical marsh and to the north the Atlantic Ocean. The Learjet was based at Zanderij airport (5.45° N and 55.17° W) approximately 50 km south of the country's capital Paramaribo and the coast. With a flight range of ~ 2000 or 4000 km total flight distance, a considerable area could be examined at various altitudes and times of the day.

HOOVER is an airborne campaign based out of Hohn in northern Germany. With a flight range of 2500 km, flights to the north can reach northern Europe (Kiruna, Sweden) and flights to the south can reach the Mediterranean (Corsica, France) with refueling at the two extremes. Flights in various seasons will give a chemical overview of the background atmosphere over Europe including the oxidative capacity of that atmosphere. HOOVER I, the first seasonal flight, occurred in October 2006 representing air over Europe in the fall. HOOVER II occurred in July 2007 representing summer air over Europe.

2 The TRISTAR instrument

The QC laser spectrometer TRISTAR (Tracer In Situ Tdlas for Atmospheric Research) is a robust and compact system which has measured trace gases in excess of 500 flight hours in a variety of field campaigns. Instrumentation on a small aircraft implies restrictions in weight, volume and total power requirement. Development of TRISTAR has resulted in an instrument requiring only 40 cm in a 19″ rack for the electronics and permeation source and the top of two half racks for the optical table with a 60 cm × 45 cm footprint. With a total weight of 125 kg (including the rack) and using 12.5 A at 28 V (excluding the pump), this system has been optimized for aircraft field experiments on small jet aircrafts. During the field experiments the aircraft platform was a Learjet 35 A, operated by GFD (Gesellschaft für Flugzieldarstellung mbH), with a total instrument payload of 1300 kg and two operators for all instruments. TRISTAR was designed to run without an operator on board. Figure 1 shows the instrument installed on the Learjet during the GABRIEL campaign in October 2005. Only one of the half racks under the instrument is required for the electronics and pump while the other contains an H_2O_2 monitor.

2.1 *Optomechanical setup*

The optical setup is similar to that reported by [18, 19] and is based on a double corner cube White cell with a base path length of 0.5 m adjusted for a 64 m folded pathlength at 128 passes. A very rigid optical layout, initially

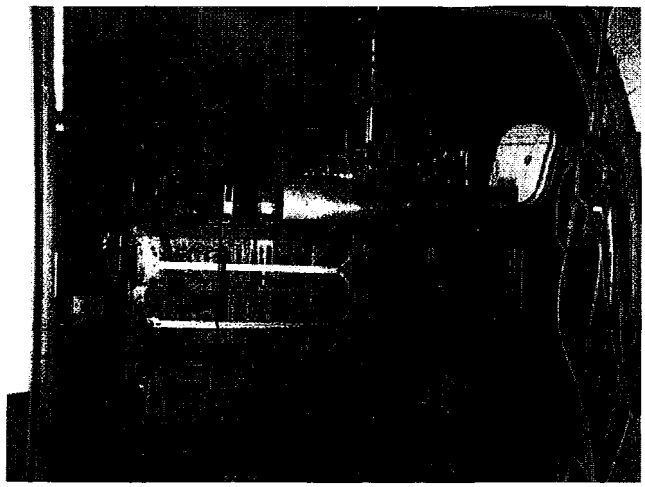

FIGURE 1 Picture of the TRISTAR onboard a Learjet 35A during the GABRIEL campaign in October 2005

developed at the Fraunhofer Institut für Physikalische Meßtechnik (Freiburg, Germany), is used for optical stability. The initial design has been modified to multiplex the lasers using two pop-down mirrors and to allow the use of an all teflon stepper valve system to control the pressure in the White cell.

The divergent QC laser beam is collected via a 26° off-axis ellipse (OAE) mirror located 44 mm from the laser ($f/2$ aperture). Through a series of flat mirrors and an off-axis parabolic (OAP) mirror, we achieve a 14 mm diameter collimated beam. A series of intermediate foci designed into the optics result in convenient alignment. The optics are actively temperature controlled to 40 ± 0.2 °C both to minimize drift of optical structures due to changes in the cabin temperature as well as to stabilize the background blackbody radiation incident on the detector. Three quantum cascade lasers (Alpes Laser, Lausanne, Switzerland) can be sequentially coupled into the White cell with use of computer controlled pneumatic pop-down mirrors.

The lasers and the detectors are housed in a single dewar and cooled with liquid nitrogen with an operating time of approximately 8 h between fills. The lasers are temperature controlled by active heating at the laser station with mK accuracy. Cooling is through a sapphire junction between a copper block in contact with the liquid nitrogen and a copper block housing the QC laser. The sapphire junction eliminates electrical contact between the laser and the housing. Due to the large heat dissipation by the QC lasers (~ 5 W), minimum temperatures achieved during operation are approximately 90 K. Therefore the lasers in use at present are temperature controlled between 90 and 120 K. Detectors for both the signal and the reference are housed within the same dewar as the lasers. The detector temperature is stable at 78.5 ± 0.5 K.

The three QC lasers used in these experiments emitted at 1268.98, 2158.30, and 1759.72 cm^{-1} and were used to measure CH_4, CO and HCHO respectively. Due to the presence of a N_2O line at 1269.29 cm^{-1} it is also possible to alternately measure N_2O and CH_4 on one channel. Since CH_4 and N_2O have long lifetimes in the atmosphere, mixing ratios are not expected to change very quickly for these species unless they are very close to an emission source (or the stratosphere) and

alternating CH_4 and N_2O measurements every 3 to 4 s give adequate resolution for both species.

2.2 *Electronics*

The electronic setup is shown in Fig. 2 and is similar to that for the QUALITAS instrument described by [15]. Experiments in the laboratory prior to GABRIEL indicated that active temperature control of the lasers was resulting in an increased noise on the laser signal. Since QC lasers are relatively insensitive to temperature tuning (approximately 2.2 GHz/K), the lasers were run with no heating, allowing an equilibrium temperature to be established due only to heating by the laser [14]. During GABRIEL it was noticed that there were rapid changes in the cabin pressure (1000 to ~ 780 mb). These changes in cabin pressure resulted in changes in temperature of liquid nitrogen and changes in the laser conditions leading to a significant change in the background spectra (see Fig. 5a). Active temperature control of the lasers was therefore reestablished during the HOOVER campaigns. Active pressure control was considered, however due to very stringent weight restrictions and could not be implemented at this time.

A saw tooth current ramp of 66 ms duration was used to sweep the laser emission line across an individual rotational-vibrational absorption line of the species of interest. Modulation of the lasers at 20 kHz with detection of the $2f$ signal at 40 kHz is used to decrease the $1/f$ noise. The design of the modulation electronics allows the phase shift on the laser current lines so that the phase is always consistent on the detector, which reduces the settling time of the lock-in amplifier as the lasers are switched between channels. Two-tone frequency modulation had been employed on a previous system, however due to high frequency pickup in-flight as well as cross talk between detectors mounted within the same station, the noise could not be reduced to acceptable levels. Therefore two-tone frequency modulation was abandoned for aircraft measurements.

After transversing the White cell, the laser light is incident on a mercury/cadmium/telluride detector (Kolmar Technologies Inc., Newburyport, MA) followed by preamplification (1000 ×) of the detector signal using a homebuilt transimpedance amplifier. This resultant signal is then demodulated using a FEMTO Meßtechnik, (model LIA-BV-150-S, Berlin, Germany) lock-in-amplifier. A simple schematic of the electronics used in TRISTAR is shown in Fig. 2.

2.3 *Data acquisition*

The data acquisition software allows significant flexibility in setting the acquisition times for individual species as well as the amount of time spent averaging each species. Since HCHO has much lower mixing ratios, near the detection limit of the instrument, longer acquisition and averaging times for HCHO are useful. In general, averaging for CO and CH_4 was between 0.7 and 1.4 s while the averaging time for HCHO was between 1.6 and 2 s. When operating on only two channels the cycle time can be controlled and dur-

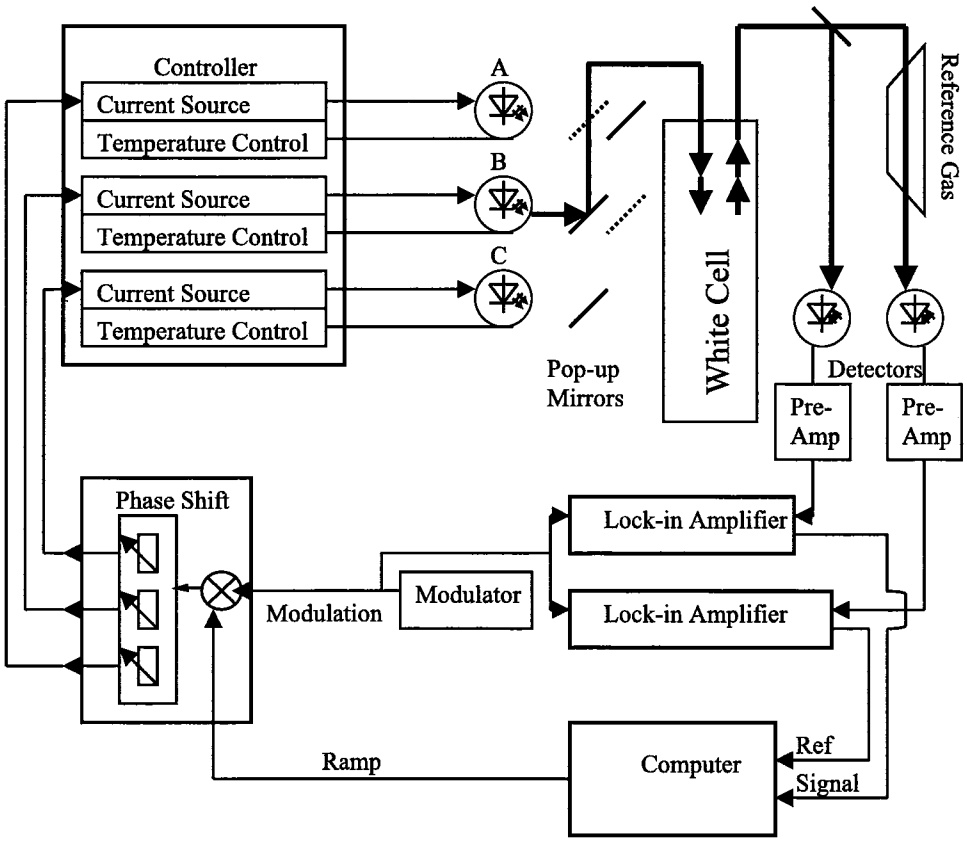

FIGURE 2 Schematic of the basic TRISTAR electronic setup

ing the GABRIEL campaign a cycle of ~ 40% CO and 60% HCHO was used. When using it as a 3-channel system such as during the HOOVER I and II campaigns, the cycle is 60% HCHO, 20% CH_4 and 20% CO.

At present, the total time associated with an ambient cycle is 19.240 s. During an ambient cycle, five spectra representing 30 averaged measurements for HCHO, and five spectra averaged from 10 measurements for both CO and CH_4 are obtained. Ambient measurement times are 9.900 s for HCHO, 3.300 s for CO and CH_4, resulting in almost 86% of the cycle spent measuring. The rest of the time is spent settling the lock-in amplifiers following channel switching. Between ambient and background measurements, a stabilization period of 15–20 s is required depending on the flow through the White cell.

2.4 *Analysis software*

Analysis software was developed using IGOR Pro (WaveMetrics) to automatically filter, subtract backgrounds if necessary, linearly fit to a calibration spectra and determine mixing ratios of a species of interest. In addition, 3D plots of the change in signal with time can be used to examine background drifts or abrupt changes in the background which can often be traced back to individual events such as a change in cabin pressure or a sharp climb or turn of the aircraft. This is extremely helpful in data quality control.

This analysis software also allows for sophisticated background subtraction as well as filtering of a spectrum of interest. Background subtraction can be a simple time based linear interpolation of the background for an ambient spectrum, or a curve fitting routine can be used for non-linear changes in the background. The latter process results in better background subtraction and thus better detection limits. However this requires much more rigorous analysis where the background structure is examined using a 3D plot of signal vs channel and time. If the background is not changing in a linear fashion it can be fit to a polynomial or other functions. In addition, abrupt changes in the background structure can be isolated and the data before or after the change treated separately. A Fourier transform of the data can also be used to filter out high frequency noise from a spectrum of interest. This can be used to efficiently remove small fringes caused by etalons within the White cell, which may not have been removed by averaging alone. This is important since etalons often change slightly with time resulting in poor subtraction and thus poor detection limits.

2.5 *Gas flow and calibration*

Ambient air was sampled from a forward facing inlet designed by enviscope GmbH. A schematic representation of the inlet system and the gas flow system is shown in Fig. 3. The forward facing stainless steel inlet is lined with thin walled 10 mm PFA tubing and is attached to a 1/2″ looped bypass line. The bypass line allows for high flows and thus low residence times within the tube. Ambient air is sampled from a short inlet line teed from the bypass line. A measured pressure drop of ~ 30–50 hPa along the bypass lines indicates a bypass flow of ~ 1000 l/min using the Hagen–Poiseuille law. However this assumes that the flow is laminar, which a Reynolds number of ~ 80 000 clearly shows it is not. A similar line was tested on another instrument and a flow of ~ 100 l/min was determined using the dilation of a calibration gas. The linear velocity is 21 m/s and the residence time within the bypass line is less than 30 ms. From the bypass line, a sample of ~ 5 slpm was withdrawn from the center of this line near to the center of flow. Residence times within this line would be ~ 40 ms.

The possibility of compressional heating due to the ram pressure of the forward facing inlet was examined. Since the inlet was a subisokinetic inlet, compressional heating would be expected. Table 1 shows the expected error in the HCHO measured at various cloud water contents assuming all the water evaporated and the HCHO in the liquid phase was released back into the gas phase. The effective Henry's law constant used in the calculation was 6.3×10^3 M atm^{-1} [20] assuming the HCHO formed the diol in solution. With a liquid water content of 1 g/m^3 which is applicable to dense low level clouds, full evaporation of the water droplets would cause a 15% error in the measured HCHO concentrations. Outside of a cloud in outflow regions, typical cloud water contents are closer to 0.01 g/m^3 [21], resulting in an estimated error in the HCHO measured of 0.15%. Therefore outside of the cloud, evaporation of the liquid water containing HCHO in equilibrium with the gas would have little effect on the measured HCHO concentration.

However, the evaporation of the droplet is a non-equilibrium process. Reference [24] shows that the time scale for equilibration of H_2O with its surroundings is on the order of 0.1 to 1 s for particles > 10 μm indicating that evaporation of the particles in the bypass line should be far from complete with a residence time of 30 ms. Therefore it is unlikely that evaporation of droplets within the sample line will have any effect on the measured HCHO mixing ratios.

Gas was sampled into the White cell via a three-way valve allowing for sampling of ambient, calibration or background gas to occur. The White cell was maintained at a constant pressure of 45 or 50 hPa, via feedback of a measured inlet pressure to control an all Teflon stepped valve at the inlet to the White cell. The stepped valve consisted of an electrically driven motor (Nanotech, labeled M in Fig. 3) moving an angled piston orthogonal to the flow, thus partially blocking the flow. Two holes of differing sizes allow for better control of the pressure over the large pressure range of operation. With a movement of the piston of 0.2 mm per turn of the screw and 400 steps per turn of the moving motor the position of the piston can be controlled by 0.5 μm steps. Flow through the White cell was limited to ~ 5 slpm via an aperture behind the cell limiting the pumping rate. Limiting the pumping rate was required to maintain the pressure of the White cell even at high altitudes when the pump is more efficient due to the lower backing pressure. With a volume of 2.7 l and a flow of 5 slpm, the residence time within the White cell is approximately 1.5 s. Flushing times for the White cell were set to 15 s between ambient, background and calibration measurements to allow for better than 99% exchange of the gas within the cells and the lines.

Backgrounds for HCHO were obtained for 25–50 s every 3–4 min. Zero air was obtained for the HCHO background and calibration by passing ambient air through a platinum on alumina converter heated to 120 °C. Flow through the scrub-

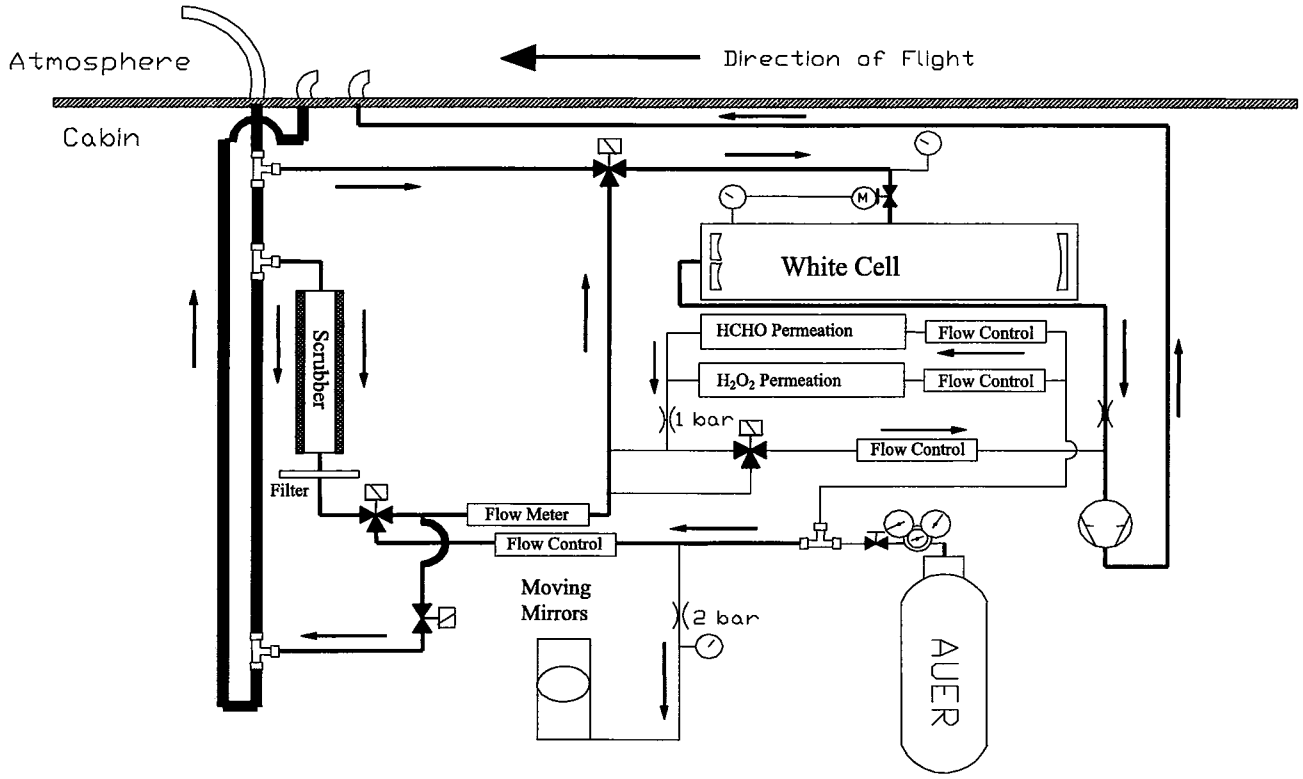

FIGURE 3 Schematic of the inlet system used during both the GABRIEL and HOOVER I campaigns

Location	Typical liquid water content (g/m^3) and references	Error estimate for HCHO measured (%)
Cb	1 [22]	15
Cu	0.2 [23]	3
Ci	0.03 [23]	0.45
Outside cloud	0.01 [21]	0.15

TABLE 1 The maximum error in measured HCHO due to evaporation of HCHO containing aerosols

ber only occurred during a background measurement. Examination of the background immediately following the flush time and at the end of the background measurements during a flight with time flowing through the scrubber showed no significant difference in the background. The scrubber efficiently removes HCHO while leaving many other gases unaffected. A 5 μm filter following the scrubber was used to remove any particulate that may be liberated from the scrubber. The efficiency of the converter was determined by introducing air spiked with 15 ppb of HCHO and measuring the breakthrough. Repetitive tests in the laboratory of more than a one-hour duration showed no measurable HCHO breakthrough. Scrubbing of an ambient air sample is preferable when possible since removal of the molecule of interest while leaving other species such as CH_4, N_2O and water vapor near their ambient levels leads to better background subtraction and thus better detection limits.

The calibration gas for CO, N_2O and CH_4 was obtained from a calibrated bottled air source. Ambient air was filtered and compressed into a 6 l carbon composite bottle (Auer GmbH) and calibrated against a NIST traceable standard in the laboratory. Mixing ratios ranged from 250–350 ppbv for CO depending on the local ambient values during compression. Methane mixing ratios were consistently between 1850–1900 ppbv while those for N_2O ranged from 280 to 380 ppbv. In flight calibrations of CO, N_2O and CH_4 generally occurred every 30–40 min.

Calibration of HCHO involved introducing a flow from a permeation source into a zero air stream of scrubbed ambient air [25]. The permeation source was a sealed wafer device (Valco Instruments Co. Inc.) in a glass tube temperature controlled to 70 °C. The 30 ml/min flow from the permeation source was either pulled off by a pump, or mixed with scrubbed ambient air to produce calibration mixing ratios ranging from 5 to 8 ppbv depending on the flow of the dilution gas. The permeation sources were held at a constant pressure of (1050 ± 0.5) mb to minimize the pressure changes within the permeation source with altitude.

3 Instrument performance

3.1 *Precision of* CO, CH_4 *and* N_2O *measurements*

CO was measured during both the GABRIEL and HOOVER campaigns. Examination of the reproducibility of in-flight calibration signals can be used to determine the precision of the measurement. Table 2 shows the precision and the optical density (OD) for CO measurements obtained during GABRIEL 2005 and HOOVER 2006 and 2007. The precision in the measurement of the calibration was better than 0.5% (2σ) for 0.7 s data and 0.3% (2σ) for 1.3 s data. The largest error in the total uncertainty is due to the uncertainty in our

reference NOAA standard for CO of 1%. The limit to the precision of the CO measurement at present is thought to be due to the stability of pressure in the White cell and is discussed in detail later in this paper.

Using the HITRAN database [26], the line center OD of the 2158.3 cm^{-1} line for 273 ppbv of CO was calculated for a Voigt line shape to be 5.38×10^{-2}. The minimum detectable OD was calculated using the 1σ precision and the precision determined in each flight and is summarized in Table 1. The GABRIEL flight was separated into flights 3–5 and flights 7–10 since the time resolution was different during these two periods. For GABRIEL flights 3–5 the average minimum OD of 7.6×10^{-5} was calculated which corresponds to a normalized detectable OD of $1.35 \times 10^{-6}\,Hz^{-1/2}\,m^{-1}$. It should be noted that with an optical density of 5% or higher, correction of the CO data for the non-linearity at high mixing ratios was required. The precision of the instrument is comparable to that achieved in [14] of 0.34%. However since the line used in [14] was 10 times smaller in line strength, the calculated minimum optical density for the instruments is considerably different. This may not indicate a significant performance difference in the instruments, but may indicate that the noise dominating the precision is from other sources such as pressure or temperature stability.

Included in Table 2 are the preflight laboratory determinations of the minimum detectable OD as determined by the precision before both the GABRIEL and HOOVER campaigns. As expected the performance of the instrument was somewhat better in the laboratory under ideal conditions. This was thought to be due to the temperature stabilization of the lasers since only passive cooling was used to control temperature during the campaign. It had been noted in laboratory studies that active temperature control of the lasers significantly increased the noise on the lasers. This may have been due to very small changes in the laser temperature due to imperfect PID settings. In the laboratory temperature and pressure remain relatively constant, however within the aircraft, temperature and pressure changes in the cabin resulted in strong drifts of the signal when under passive temperature control. This explains the decreased performance of the instrument during flights compared to its preflight laboratory sensitivity. Unregulated cooling was abandoned during HOOVER as a result. Advances in temperature control of the optics and pressure control of the laser dewar may result in a decrease in this drift and allow passive cooling alone for temperature control of the lasers in the future or better heating control may be required to reduce the noise associated with active temperature control.

Table 3 shows the precision and optical densities determined for CH_4 measured during the HOOVER I and II field experiments. The precision in the measurement of our calibration was approximately 0.8% (2σ) during HOOVER I and improved to 0.61% for HOOVER II for 0.7 s measurement. The uncertainty of the reference NOAA standard for CH_4 was very good resulting in a total uncertainty of the calibration standard of 0.4% (2σ). Using a Voigt line shape, the OD of a 1903.3 ppbv line at 1268.98 cm^{-1} is 4.13×10^{-2} as calculated using the Hitran 2000 database [26]. Due to the large optical densities at these mixing ratios, correction for the non-linearity at this high absorption is required. A detectable OD of 1.5×10^{-4} was calculated using the 1σ precision of 6.9 ppbv, which corresponds to a normalized detectable OD of $2.8 \times 10^{-6}\,Hz^{-1/2}\,m^{-1}$. The precision of methane measurements in the 1269 cm^{-1} region was consistently poorer than that for the CO in the 2159 cm^{-1} region. This may be due to the influence of the water vapor lines and bands in the 1269 cm^{-1} region. However, the likely cause of the reduced precision for CH_4 is due to the effect of pressure on the line widths since CH_4 at longer wavelengths has more Lorentzian characteristics (further from the Doppler limit) than does CO, resulting in a greater line width dependence on pressure. This indicates that measuring only on and off line center may result in better precision of these measurements than fitting to the entire line. The effect of pressure on the line width is discussed in the next section.

During HOOVER II, measurements of N_2O were alternated with measurements of CH_4. This did not appear to have an effect on the CH_4 measurements other than reducing the total number of measurements. Table 4 shows the precision and optical densities determined for N_2O measured during

Flight	Time resolution (s)	1σ standard deviation (ppbv)	95% confidence precision (%)	1σ minimum OD ($\times 10^{-4}$)	1σ normalized minimum OD ($\times 10^{-6}\,Hz^{-1/2}\,m^{-1}$)
Pre-GABRIEL Lab	1.3	0.18	0.33	0.35	0.63
GABRIEL (1, 3–5)	1.3	0.39	0.28	0.76	1.35
GABRIEL (7–10)	0.7	0.64	0.48	1.26	1.64
Pre-HOOVER Lab	0.7	0.62	0.41	1.22	1.54
HOOVER I	0.7	0.67	0.56	1.32	1.67
HOOVER II	0.7	0.87	0.76	1.71	2.23

TABLE 2 Precision and uncertainty in CO measurements during GABRIEL 2005 and HOOVER I and II. The minimum optical density is calculated for a 64 m pathlength and the time resolution shown

Flight	Time resolution (s)	1σ standard deviation (ppbv)	95% confidence precision (%)	1σ minimum OD ($\times 10^{-4}$)	1σ normalized minimum OD ($\times 10^{-6}\,Hz^{-1/2}\,m^{-1}$)
HOOVER I	0.7	6.9	0.72	1.5	1.9
HOOVER II	0.7	5.7	0.61	1.2	1.6

TABLE 3 Precision and uncertainty in CH_4 measurements during HOOVER I and II. The minimum optical density is calculated for a 64 m pathlength and the time resolution shown

Flight	Time resolution (s)	1σ standard deviation (ppbv)	95% confidence precision (%)	1σ minimum OD ($\times 10^{-4}$)	1σ normalized minimum OD ($\times 10^{-6}$ Hz$^{-1/2}$ m^{-1})
HOOVER II	0.7	0.87	0.54	0.81	1.1

TABLE 4 Precision and uncertainty in N_2O measurements during HOOVER II. The minimum optical density is calculated for a 64 m pathlength and the time resolution shown

the HOOVER II field experiment. The precision in the measurement of our calibration was approximately 0.54% (2σ) during HOOVER II for 0.7 s measurement. Using a Voigt line shape, the OD of a 315 ppbv line at 1269.28 cm^{-1} is 2.95×10^{-2} as calculated using the Hitran 2000 database [26]. Due to the large optical densities at these mixing ratios, correction for the non-linearity at this high absorption is also required for N_2O. A detectable OD of 8.1×10^{-5} was calculated using the 1σ precision of 0.87 ppbv, which corresponds to a normalized detectable OD of 1.1×10^{-6} Hz$^{-1/2}$ m^{-1}. The precision and detection limits for this line were very good for dry air, however at low altitudes a water line present very close to the N_2O line required correction of the data for water and resulted in much poorer precisions. Although the best line pairs used for the simultaneous measurement of CH_4 and N_2O were not ideal, they did show proof of principle making alternate measurements of CH_4 and N_2O on the same laser possible with little effect to the precision of the method.

During HOOVER II on one of the flight legs (flight 2 – north) a region of very well mixed air was encountered. This allowed us to determine precisions of our instrument from actual ambient data. Precision at 95% confidence for CO was 0.45%, for CH_4 was 1.06% and for N_2O was 0.57%. The precision for CO and N_2O were comparable to those calculated from replicate calibrations however the precision of CH_4 was considerably larger.

3.2 *Pressure dependence on* CO *and* CH_4 *measurements*

It has been suggested that pressure fluctuations may be the largest sources of error in the measurements of CO, CH_4 and N_2O [15]. Calculation of the optical density at various pressures can indicate the sensitivity to pressure under the operating conditions. A calibration at 50 mb was carried out followed by incremental changes in the pressure. Figure 4a shows the measured change in mixing ratio as a function of pressure. The resultant curve is the apparent mixing ratio of CO as a function of the measurement pressure. Figure 4b shows the calculated optical density at line center as a function of pressure for CO as calculated using the HITRAN 2000 database [26]. The change in measured apparent CO as a function of pressure indicates a 1.4% per mb dependence, while the calculation using the Voigt line shape to determine the pressure dependence on the OD at line center yields a 0.8% per mb change in the OD. However line width is also affected by changes in pressure since the Lorentzian line width and therefore the Voigt line width is directly proportional to the pressure. Changes in the line width result in an increased error in the fit, and thus can be as significant as the changes in the line center. With a 1σ fluctuation of the pressure of 0.5 mb, we would expect a corresponding effect on the precision to be 0.7%. Therefore with precisions ranging from 0.3 to 0.6%, the majority of this fluctuation can be attributed to the pres-

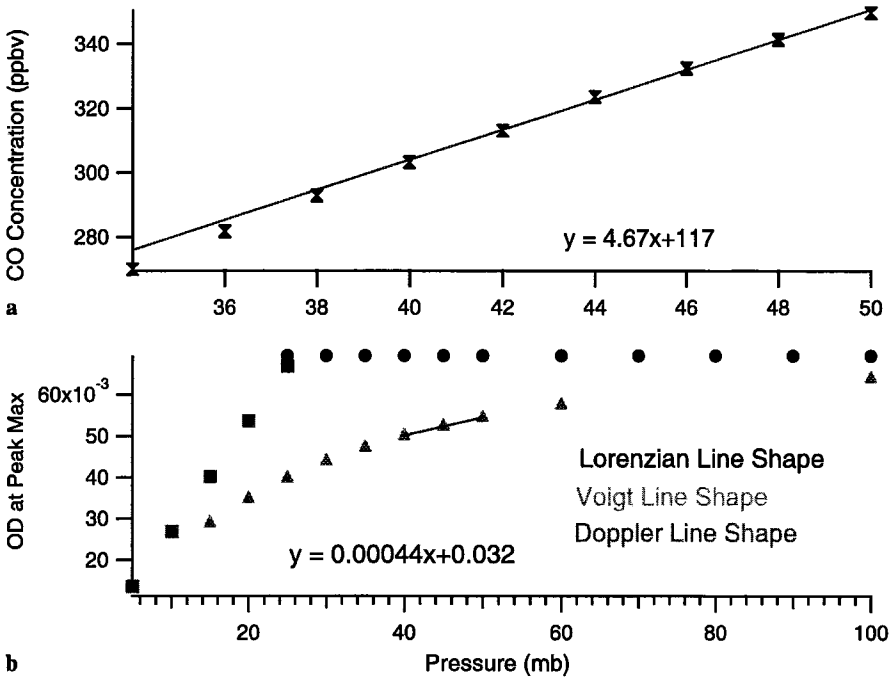

FIGURE 4 (**a**) The apparent CO mixing ratio measured as a function of pressure when calibrated at 50 mb pressure. (**b**) The optical density at peak center for CO as calculated using the Lorentzian (*circle*), Voigt (*triangle*) and Doppler (*square*) line shapes

sure. A similar calculation for methane showed the measured fluctuation to be 1.25% per mb.

3.3 *Measurement of* HCHO, *precision and analysis of detection limit methods*

Unlike CO, CH_4 and N_2O, formaldehyde mixing ratios tend to be low and often are measured near instrument detection limits. In order to reduce the detection limits, various methods such as averaging and background subtraction have been used [27]. Background subtraction can reduce the detection limit by eliminating structures in the scan across an absorption line that are not due to the absorption by HCHO or the molecule of interest. These may include interferences by other molecules and changes in the laser power across the scan. The interfering molecules often include species such as H_2O, which may have very large bands within a region thereby affecting the background of a species. Additionally, optical noise, so called etalon fringes, often arise due to back-reflections between distinct elements of the optical path, that give rise to undulating signals superimposed on the absorption structure under investigation. Therefore, by subtracting a background of ambient air from which all the HCHO has been removed, all that remains is the signal due to the presence of HCHO. However, since simultaneous background and ambient measurements cannot be made, there may be a drift in the background conditions possibly due to drifts in pressure within the White cell or drifts in temperature of the optics resulting in minute changes in the optical path through the White cell and therefore the noise. Thus reduction of pressure, both White cell and cabin, and temperature fluctuations are important in the stability of the background structure. This is readily apparent by comparing Fig. 5a and b. Figure 5a is a three dimensional plot of all data taken during a flight before background subtraction. Time is on the x-axis, and the 256 channels that are scanned across are on the y-axis, while the color scale in the z-axis indicates the strength of the signal. The bluer the signal, the more positive the number with respect to the median while the redder the signal, the more negative the number. We can see that there is considerable drift of an etalon fringe in Fig. 5a, however drift of an etalon fringe in Fig. 5b is considerably reduced. Also included in Fig. 5b is a temperature measurement of a portion of the optical plate very near the laser input. We can see that there is a clear change in the signal when the heater turns on and there is a rapid change in the temperature. Temperature stabilization of the optics is important to minimize the change in the signal and optimize background subtraction. Other abrupt changes can be attributed to such things as cabin pressure changes and changes in the acceleration of the aircraft.

Reproducibility of the background resulted in a 1σ standard deviation for a 1.65 s integrated measurement of 0.71 ppbv during the first half of the flights during GABRIEL decreasing to 0.45 ppbv using a 1.98 s integration time during the later half of the flights (Table 5). Increasing the averaging to 120 s of elapsed time decreased this detection limit to 340 and 130 pptv respectively at 1σ. Since only a small fraction of this time is spent on backgrounds during this 120-s time average, a true $\sqrt{N}$ reduction of the detection limit is not achieved. Averaging 120 s of background results in a detection limit calculated to be 53 pptv, as would be expected by a $\sqrt{N}$ reduction in the noise. Detection limits were similar during HOOVER I and II. Using the reproducibility of backgrounds for the detection limit may overestimate the detection limit due to slow changes in the background structure that can be accounted for between backgrounds.

A filter of the data for small etalon fringes was tried. The filter utilizes a Fourier transform to remove small high-frequency fringes. Examination of filtering of the results shows little gain in the detection limit when averaging for 2 s, however a slight decrease in the detection limit was noted for some of the flights. It should be noted that using the filter on flights with little or no etalon structure appeared to have little effect on the calculated concentrations.

Detection limits have also been calculated by determining the variance of a plot at the integration time interval of measurement from an Allan variance plot [28, 29]. Figure 6 shows the Allan variance as a function of time for a 6 ppbv standard calibration. With only 15 min of data, averages longer than 100 s resulted in very few points and thus are less reliable variances. In addition, not enough time was available in order for the longer time scale drifts to become apparent. However it should be noted that the system is stable past 100 s, which shows improvement from previous setups [19]. If averaging to 120 s, then the variance would be equal to approximately 0.004 and thus the standard deviation would be 63 pptv indicating a detection limit at approximately 63 pptv for a 120 s average. However since the cycle is only $\sim$ 60%, using a 70 s averaging time may be more appropriate, which results in a detection limit of 90–100 pptv. This is very similar to the detection limit determined by using the reproducibility of the blanks.

Detection limits were also estimated by determining the standard deviation of measurements in relatively clean air and

Flight	Time resolution (s)	1σ standard deviation (ppbv)	1σ minimum OD ($\times 10^{-5}$)	1σ standard deviation for 120 s average (ppbv)	1σ minimum OD 120 s resolution ($\times 10^{-6}$)	1σ normalized minimum OD ($\times 10^{-7}$ $Hz^{-1/2}$ m^{-1})
GABRIEL (1, 3–5)	1.65	0.71	2.80	0.34	13.5	5.7
GABRIEL (7–10)	1.65	0.45	1.82	0.13	5.0	3.6
HOOVER I no filtering	1.98	0.56	2.26	0.18	7.5	5.0
HOOVER I filtering	1.98	0.56	2.20	0.15	5.5	5.0
HOOVER II	1.98	1.64	2.58	0.032	1.28	5.67

TABLE 5 Detection limits in HCHO measurements during GABRIEL 2005 and HOOVER I and II

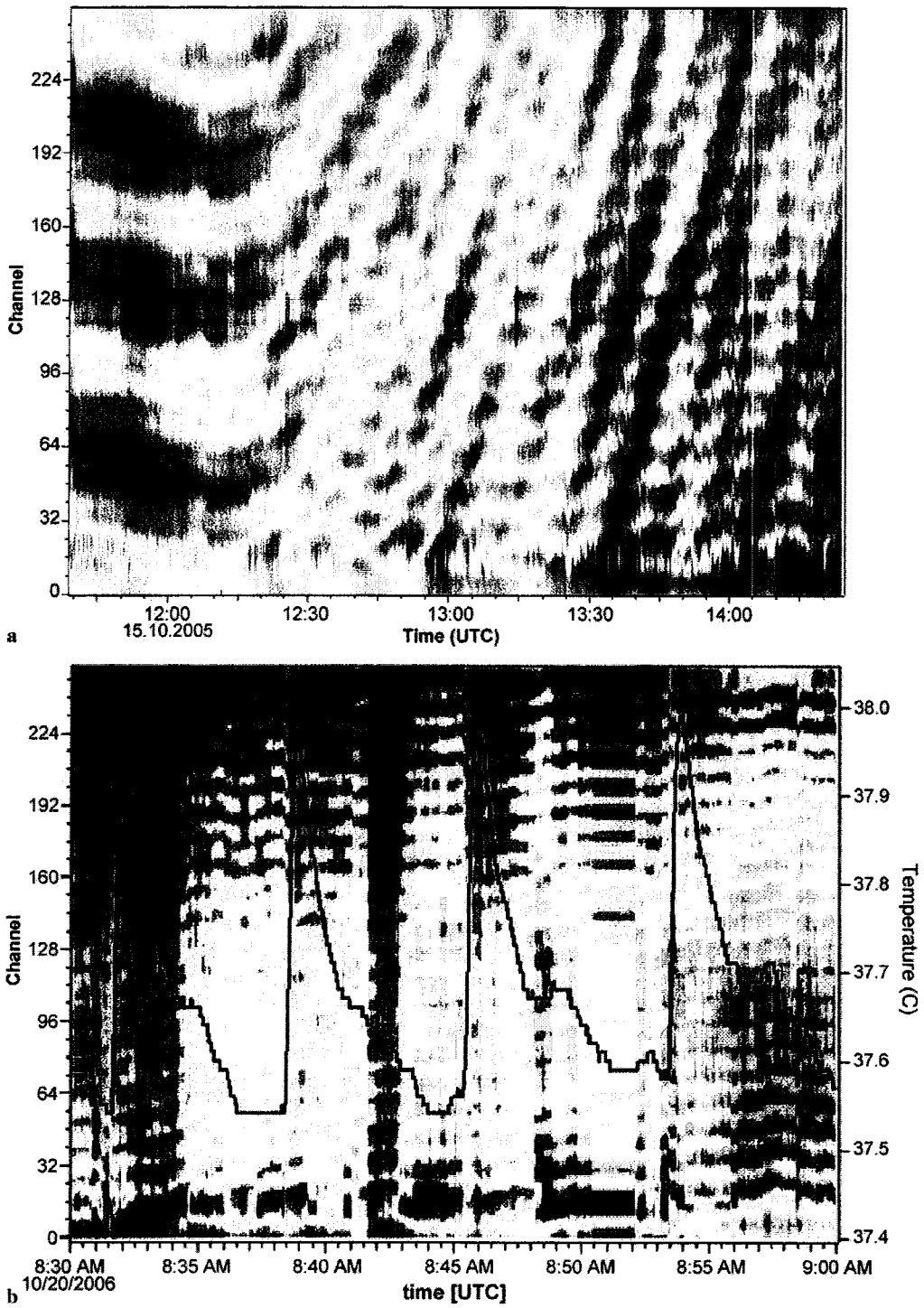

FIGURE 5 (**a**) All measurements from GABRIEL flight 10 for HCHO are shown. The channels scanned (256 in total) are shown in the *y*-axis, with the intensity as a color-coding in the *z*-axis. The color-coding is such that the blue indicates a higher number while the red a lower number about a median value. (**b**) All ambient measurements from HOOVER I flight 2a for HCHO are shown. The channels scanned (256 in total) are shown in the *y*-axis, with the intensity as a color-coding in the *z*-axis. The temperature measured on the optical table is shown as a *dark trace* with its corresponding scale on the right vertical axis

dividing by the square root of the number of measurements in the averaged interval [30]. In these cases, the standard deviations of very low measured mixing ratios of HCHO is obtained during situations where the air mass is relatively well mixed and not changing significantly with time. During GABRIEL these air masses were observed over the ocean above the boundary layer. During HOOVER these air masses could be found above the boundary layer in northern Europe well removed from anthropogenic influences. As an indicator, CO concentrations below 80 ppbv and varying only a few ppbv were the criteria. During HOOVER II, one such event occurred for close to 20 min with the CO 1σ standard deviation being 0.55 ppbv for the whole flight level. During GABRIEL flight 8, a standard deviation of 136 pptv for 11 consecutive measurements yielded a detection limit of 41 pptv and during flight 9 a similar calculation was made for 14 points yielding a detection limit of 37 pptv. During HOOVER II the concentration of HCHO during a 20 min leg was 41 ± 550 pptv for a 1 s average. During the 120 s 29 points were obtained resulting in a detection limit of 100 pptv. This is

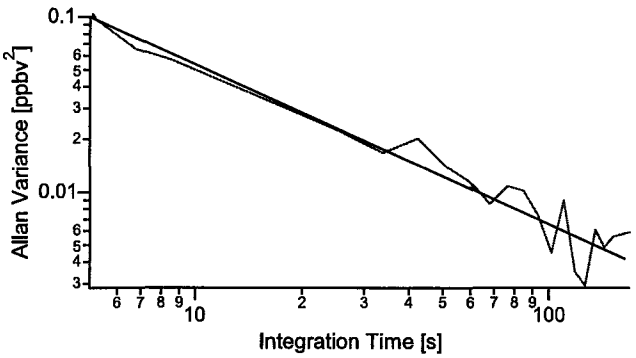

FIGURE 6 Allan plot of TRISTAR measurements in the laboratory for a 6 ppbv calibration standard. The time indicated is the averaging time on the HCHO channel including stabilization times

similar to a detection limit of 133 pptv obtained for flight 8 or the 87 pptv obtained for flight 9 when calculating the detection limit as the standard deviation of the backgrounds. This would be comparable to a 46 pptv detection limit when utilizing a 100 m Herriot cell and are thus comparable to the 15–50 pptv detection limit obtained by Fried et al. [3] during TRACE-P 2001. All three methods result in detection limits that agree within a factor of two, with the largest obtained using reproducibility of the backgrounds while the standard deviation of low concentrations of HCHO results in the lowest. This indicates that drift of the backgrounds accounts for a significant increase in the detection limit and that reducing the fluctuation of the background or taking more frequent backgrounds should significantly improve the detection limit.

4 Airborne measurements

Figure 7 shows the measurement of HCHO and CO as a function of time during flight 8 of the GABRIEL campaign in October 2005. As expected the mixing ratios within the boundary layer were considerably higher than those in the free troposphere for both species. In the free troposphere, the mixing ratios for HCHO were near the detection limit of 130 pptv while within the boundary layer the values for HCHO were considerably higher ranging from 1.5 to 2.5 ppbv. The mixing ratio of HCHO was dependent upon the distance from the coast, with higher mixing ratio inland. See [1] for a comprehensive discussion.

Figure 8 shows the correlation between CO and HCHO during flight 8. The triangles indicate air that was below 2 km near the coast, the circles indicate air below 2 km inland from the coast, both of which were within the boundary layer. The squares indicate measurements obtained at altitudes above 3.5 km and therefore are likely measurements taken in the free troposphere where trace gas mixing ratios are generally much lower. Examination of the data indicates a slight correlation between CO and HCHO in the boundary layer, but no correlation within the free troposphere. Since both CO and HCHO are products of hydrocarbon oxidation, a correlation between them near the hydrocarbon source region would be expected. Since the boundary layer contains numerous sources for hydrocarbons, one would expect this correlation within the boundary layer. However above the boundary layer in the free troposphere a correlation between the two is less likely due to the significantly different lifetimes of CO and HCHO. A closer examination of the data reveals that the correlation inland is different from that near the coast. The inland section boundary layer measurements are represented by circles and show a correlation of 0.020 ppbv/ppbv ($r^2 = 0.63$). This is significantly larger than seen during INDOEX over the Indian Ocean where a 0.0032 ppbv/ppbv slope was observed [17], however it is also much lower than observed during MINATROC in Tenerife (0.0425 ppbv/ppbv) [19]. It is interesting to note that this production value is very close to the 0.026 ppbv/ppbv observed from a controlled burn in North Carolina [31]. The coastal section boundary layer measurements are represented by triangles and show a correlation of 0.078 ppbv/ppbv ($r^2 = 0.83$). This was measured near the city of Paramaribo, which could show an increased oxidation of NMHC in the presence of NO_x in this region.

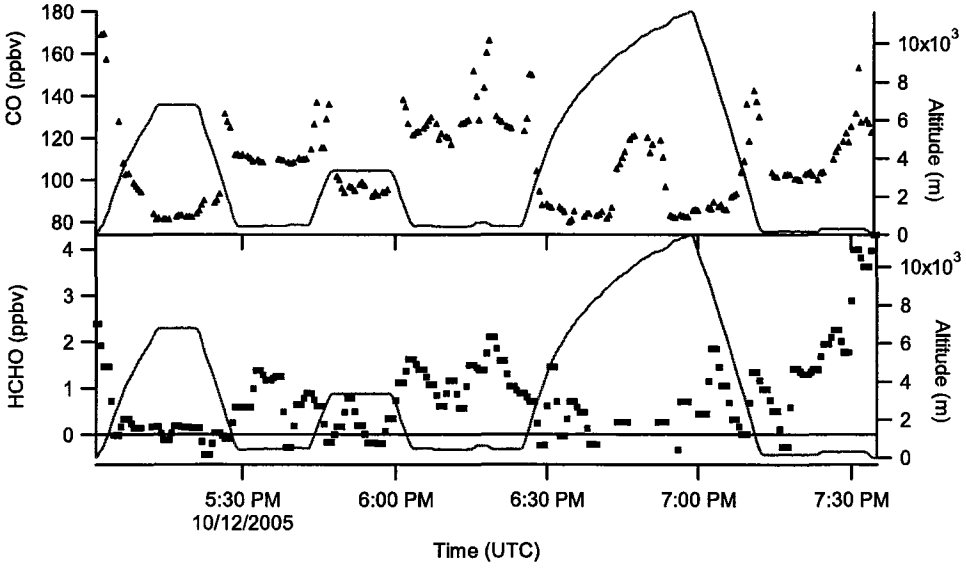

FIGURE 7 CO and HCHO mixing ratios measured on a flight during the GABRIEL 2005 campaign

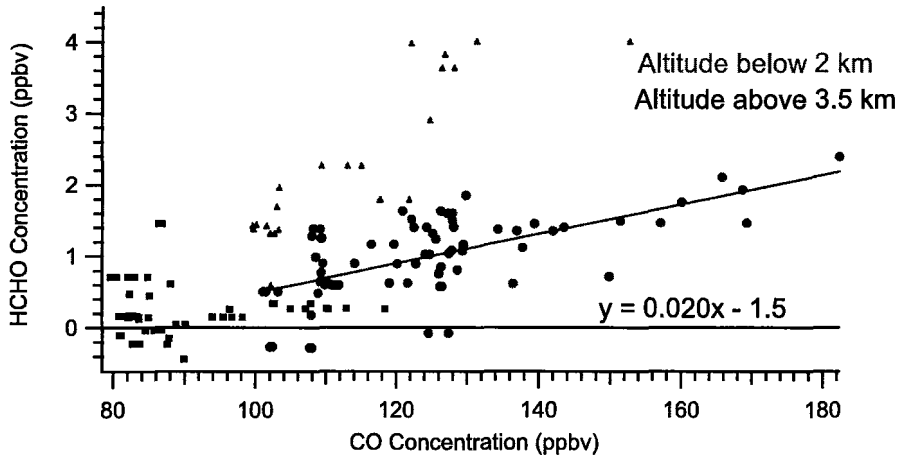

FIGURE 8 Correlation of CO vs HCHO mixing ratios from flight 8 of GABRIEL 2005. The *triangles* represent data below 2 km in height near the coast while the *circles* are also below 2 km in height but are inland from the coast. The *squares* represent data measured above 3.5 km representing air in the free troposphere

5 Summaries and future work

Improvements of TRISTAR have been realized making it very useful as a multi-species measurement tool for airborne measurements. It is smaller and lighter than past versions and continual increases in its sensitivity have resulted in an instrument that is useful for measurements within both a polluted boundary layer as well as in a clean marine boundary layer, the free troposphere or the lower stratosphere. Since this system measures three to four species by the use of pop-down mirrors, it will likely never be as stable as a system focused solely on one species, however it is very useful for aircrafts with limited payload space, weight and power restrictions. Combined with the fact that the instrument requires minimal operator support during a flight results in an instrument that is suitable for use in high-flying aircraft such as HALO (high altitude and long range aircraft).

Precisions of 0.5, 0.5 and 0.7% have been realized for 1-s measurement of CO, N_2O and CH_4. This level of precision is useful for determinations of air mass origin and transport pathways due to ratios of various species with CO and/or CH_4 and N_2O such as those originating from biomass burning. In the future the system could be utilized for eddy correlation measurement of fluxes both from an aircraft as well as on the ground.

Measurement of HCHO has been added to the TRISTAR capabilities in the past two years to take advantage of the significant improvements in the stability of the system. Detection limits were calculated using Allan variance, comparisons of replicate precisions under constant air mass periods as well as variations in the background measurements. Determination of the detection limit by fitting to the residual of replicate backgrounds resulted in a 1σ detection limit for 2 s averaging a range of 400 to 650 pptv. When averaged to 120 s, the detection limit ranged from ~ 100 to 200 pptv. The Allan variance approach also resulted in a detection limit estimate of approximately 100 pptv, while the detection limit determined as the precision of ambient air measured under constant air mass conditions was significantly lower at 50–100 pptv.

Although significant modifications have been made to the instrument, there is room for improvement. Reduction of size and weight of the instrument is always important in an airborne instrument. Digital lock-in-amplifiers coupled with new computing capabilities will decrease the weight and size of the instrument further while increasing the ramp speed due to lower time constants on the lock-in-amplifier. Maintaining constant pressure in the laser dewar will also be implemented to decrease the cooling changes due to cabin pressure fluctuations. Use of room temperature QCL lasers will also be implemented in the near future. Heating of the optics are being modified to decrease the rapid changes in the implemented scheme to increase the temperature stability of the optics. Changing the inlet section of the White cell is expected to result in better pressure control as well as increasing the flow through the cell. Better pressure control of the White cell pressure should increase the precision of CO and CH_4. The increased flow through the White cell will decrease the residence time and therefore the flush times of the cell. Decreasing the flush times can increase the frequency of backgrounds without loss of ambient measurement time. Implementation of these should decrease the detection limit for HCHO as well as improve the precision for CO, CH_4 and N_2O.

ACKNOWLEDGEMENTS The authors would like to thank all the GABRIEL and HOOVER teams for their hard work, cooperation and enthusiasm in making the GABRIEL and HOOVER campaigns a success. The authors would especially like to thank enviscope GmbH and GFD for doing everything possible for us to obtain our goals during the GABRIEL and HOOVER campaigns.

REFERENCES

1 A. Stickler, H. Fischer, H. Bozem, C. Gurk, C. Schiller, M. Martinez-Harder, D. Kubistin, H. Harder, J. Williams, G. Eerdekens, N. Yassaa, L. Ganzeveld, R. Sander, J. Lelieveld, Atmosph. Chem. Phys. **7**, 3933 (2007)

2 A. Fried, Y. Wang, C. Cantrell, B. Wert, J. Walega, B. Ridley, E. Atlas, R. Shetter, B. Lefer, T.M. Coffey, J. Hannigan, D. Blake, N. Blake, S. Meinardi, B. Talbot, J. Dibb, E. Scheuer, O. Wingenter, J. Snow, B. Heikes, D. Ehhalt, J. Geophys. Res. **108**, 8365 (2003)

3 A. Fried, J. Crawford, J. Olson, J. Walega, W. Potter, Z.B. Wert, C. Jordan, B. Anderson, R. Shetter, B. Lefer, D. Blake, N. Blake,

S. Meinardi, B. Heikes, D. O'Sulivan, J. Snow, H. Fuelberg, C.M. Kiley, S. Sandholm, D. Tan, G. Sachse, H. Singh, I. Faloona, C.N. Harward, G.R. Carmichael, J. Geophys. Res. **108**, 8798 (2003)
4 C.L. Schiller, S. Locquiao, T.J. Johnson, G.W. Harris, J. Atmosph. Chem. **40**, 275 (2001)
5 G.I. Mackay, D.R. Karecki, H.I. Schiff, J. Geophys. Res. **101**, 14721 (1996)
6 P. Werle, B. Scheumann, J. Schandl, Opt. Eng. **33**, 3093 (1994)
7 G.W. Harris, D. Klemp, T. Zenker, J.P. Burrows, B. Mathieu, J. Atmosph. Chem. **15**, 315 (1992)
8 H. Schiff, D.R. Hastie, G.I. Mackay, T. Iguchi, B.A. Ridley, Environ. Sci. Technol. **17**, 352 (1983)
9 H. Schiff, G. Mackay, J. Bechera, *Air Monitoring by Spectroscopic Techniques* (Wiley, New York, 1994), Vol. 127
10 D. Brassington, Adv. Spectrosc. **24**, 83 (1995)
11 M. Tacke, F. Weinhold, R. Grisar, H. Fischer, F.-J. Lübken, *Air Monitoring by Tunable Mid-infrared Diode* (Wiley, New York, 2000), p. 2033
12 F.K. Tittel, D. Richter, A. Fried, Top. Appl. Phys. **89**, 445 (2003)
13 C.R. Webster, G.J. Flesch, D.C. Scott, J.E. Swanson, R.D. May, W.S. Woodward, C. Gmachl, F. Capasso, D.L. Sivco, J.N. Baillargeon, A.L. Hutchinson, A.Y. Cho, Appl. Opt. **67**, 411 (1998)
14 C. Mann, Q.K. Yang, F. Fuchs, W. Bonner, R. Kiefer, K. Köhler, H. Schneider, R. Kormann, H. Fischer, T. Gensty, W. Elsäßer, Adv. Solid State Phys. **43**, 351 (2003)
15 R. Kormann, R. Königstedt, U. Parchatka, J. Lelieveld, H. Fischer, Rev. Sci. Instrum. **76**, 075 102 (2005)
16 G.J. Frost, M. Trainer, G. Allwine, M.P. Buhr, J.G. Calvert, C.A. Cantrell, F.C. Fehsenfeld, P.D. Goldan, J. Herwehe, G. Hubler, W.C. Kuster, R. Martin, R.T. McMillen, S.A. Montzka, R.B. Norton, D.D. Parrish, B.A. Ridley, R.E. Shetter, J.G. Walega, B.A. Watkins, H.H. Westberg, E.J. Williams, J. Geophys. Res. **103**, 22491 (1998)
17 V. Wagner, C. Schiller, H. Fischer, J. Geophys. Res. **106**, 28529 (2001)
18 F.G. Wienhold, H. Fischer, P. Hoor, V. Wagner, R. Königstedt, G.W. Harris, J. Anders, R. Grisar, M. Knothe, W.J. Riedel, F.-J. Lübken, T. Schilling, Appl. Phys. B **67**, 411 (1998)
19 R. Kormann, H. Fischer, C. Gurk, F. Helleis, T. Klüpfel, K. Kowalski, R. Königstedt, U. Parchatka, V. Wagner, Spectrochim. Acta A **58**, 2489 (2002)
20 J.H. Seinfeld, S.N. Pandis, *Atmospheric Chemistry and Physics: From Pollution to Climate Change* (Wiley, Toronto, 1998)
21 R.J. Weber, A.D. Clarke, M. Litchy, J. Li, G. Kok, R.D. Schillawski, P.H. McMurry, J. Geophys. Res. **103**, 28337 (1998)
22 R.D. Borys, M.A. Wetzel, Bull. Am. Meteorol. Soc. **78**, 2115 (1997)
23 D. Rosenfeld, I.M. Lensky, Bull. Am. Meteorol. Soc. **79**, 2457 (1998)
24 H. Xue, A.M. Moyle, N. Magee, J.Y. Harrington, D. Lamb, J. Atmosph. Sci. **62**, 4310 (2005)
25 F.P. Scaringelli, A.E. O'Keefe, E. Rosenberg, J.P. Bell, Anal. Chem. **42**, 871 (1970)
26 L.S. Rothman, A. Barbe, D. Chris Benner, L.R. Brown, C. Camy-Peyret, M.R. Carleer, K. Chance, C. Clerbaux, V. Dana, V.M. Devi, A. Fayt, J.-M. Flaud, R.R. Gamache, A. Goldman, D. Jacquemart, K.W. Jucks, W.J. Lafferty, J.-Y. Mandin, S.T. Massie, V. Nemtchinov, D.A. Newnham, A. Perrin, C.P. Rinsland, J. Schroeder, K.M. Smith, M.A.H. Smith, K. Tang, R.A. Toth, J. Vander Auwera, P. Varanasi, K. Yoshino, J. Quant. Spectrosc. Radiat. Transf. **82**, 5 (2003)
27 P.W. Werle, P. Mazzinghi, F.D. Amato, M. De Rosa, K. Maurer, F. Slemr, Spectrochim. Acta A **60**, 1685 (2004)
28 P. Werle, R. Muecke, F. Slemr, Appl. Phys. B **57**, 131 (1993)
29 D.W. Allan, Proc. IEEE **54**, 221 (1966)
30 B.P. Wert, A. Fried, S. Rauenbuehler, J. Walega, B. Henry, J. Geophys. Res. **108**, 4350 (2003)
31 R.J. Yokelson, J.G. Goode, D.E. Ward, R.A. Susott, R.E. Babbitt, D.D. Wade, I. Bertschi, D.W.T. Griffith, W.M. Hao, J. Geophys. Res. **104**, 30109 (1999)